Impact of non-linear internal waves on the mixed-layer heat budget along the continental slope and shelf region off Peru

Bachelor's Thesis

in the program (B.Sc) **Physik des Erdsystems - Meteorologie, Ozeanographie, Geophysik**
Faculty of Mathematics and Natural Sciences
Christian-Albrechts-University, Kiel

Author:
Thilo Klenz
Matriculation number: 1005607

Supervisor: Dr. Marcus Dengler
Second assessor: Dr. Johannes Karstensen

Kiel, June 2014

Contents

1 Abstract

1.1 Abstract

This work gives an estimate of the impact of non-linear internal waves (NLIWs) on the mixed-layer heat budget in the eastern Pacific along the continental slope and the Peruvian shelf region.
During the Meteor 92 research (M92), from January 5^{th} 2013 until January 31^{st} 2013, turbulent kinetic energy dissipation below the mixed-layer and in the water column was measured using microstructure sondes. By defining two mean states, one, when NLIWs were present, and another, during which time no NLIWs were observed, the impact of these wave events, characterized by enhanced rates of dissipation and large diapycnal heat fluxes beneath the mixed-layer, on the mixed-layer heat budget will be analysed. Further, using acoustic Doppler current profiler (ADCP) data to detect NLIW events, net cooling of the mixed-layer will be analysed directly using thermosalinograph data, recorded during that same cruise.
The results from both of these analyses indicate a major impact of NLIWs on the mixed-layer heat budget. Average heat fluxes below the mixed-layer during NLIW events were 60 times higher than background conditions. Single NLIW events resulting in heat fluxes in excess of $2000 W m^{-2}$ were observed. Analysis of TSG data reveiled a mean net cooling of the mixed-layer of about -0.038°C. Further analysis shows that the heat flux induced by turbulence through NLIWs accounts for over 80% of the total diapycnal heat flux below the mixed-layer, compensating for over 100% of the net surface heat flux over the continental shelf.

1.2 Zusammenfassung

In dieser Arbeit soll der Einfluss nicht-linearer interner Wellen (NLIW) auf das Wärmebudget der Deckschicht des östlichen Pazifiks auf dem Kontinentalabhang und in der Schelfregion vor Peru abgeschätzt werden.
Während der Meteor 92 Forschungsfahrt (M92), vom 05. Januar 2013 bis zum 31. Januar 2013, wurde anhand von Mikrostrukturmessungen die Dissipation von turbulenter kinetischer Energie unterhalb der Deckschicht und der darunterliegenden Wassersäule gemessen. Mit Hilfe von zwei mittleren Zuständen, einem, während NLIW vermessen wurden und wiederum eines Hintergrundzustandes, wenn keine Wellenereignisse beobachtet wurden, soll der Einfluss NLIW induzierter erhöhter Dissipationsraten und diapyknischer Wärmeflüsse unterhalb der Deckschicht auf das Wärmebudget der Deckschicht untersucht werden. Des Weiteren werden mit akkustischen Doppler-Strömungsmesserdaten nicht-lineare Wellenereignisse untersucht und die Abkühlung der Deckschicht durch Thermosalinographdaten direkt abgeschätzt.
Die Ergebnisse beider Untersuchungen führen zu dem Schluss, dass NLIW einen erheblichen Einfluss auf das Deckschicht-Wärmebudget haben. So waren Wärmeflüsse während NLIW-Ereignissen im Schnitt etwa 60mal höher als der Hintergrundzustand. Einzelne Wellenereignisse resultierten in Wärmeflüssen von über $2000 W m^{-2}$. Die Untersuchng der Thermosalinographdaten ergibt eine mittlere Abkühlung der Deckschicht während eines NLIW-Ereignisses von etwa -0.038°C. Weitere Analysen zeigen, dass der Wärmetransport durch NLIW einen Anteil von über 80% am gesamten diapyknischen Wärmetransport unter der Deckschicht hat und damit über 100% des angepassten Netto Oberflächenwärmeflusses kompensieren.

2 Introduction

2.1 Motivation

During the Meteor 92 cruise from January 5^{th} until January 31^{st} off the coast of Peru, numerous packets of non-linear internal waves moving shoreward across the continental shelf were observed using acoustic backscatter amplitudes from the ship's vessel-mounted ADCP (VADCP). Measurements of turbulent kinetic energy dissipation revealed significantly enhanced rates during NLIW events compared to measurements made when no waves were present. These observations suggest large heat fluxes beneath the mixed-layer induced by NLIWs, as previously observed by e.g. *Moum et al.* [2007] off the coast of Oregon, *Shroyer et al.* [2010] on the New Jersey shelf or *Schafstall et al.* [2010] off Mauretania. The regular occurrence of these events implies a major impact of (NLIW-induced) diapycnal heat fluxes on the mixed-layer heat budget, as quantified by *Hummels et al.* [2013] in the Atlantic cold tongue.
To better understand the role of non-linear internal waves and their impact on the mixed-layer heat budget in the Peruvian upwelling region, the contribution of NLIWs to sub-mixed-layer diapycnal heat fluxes needs to be quantified.

2.2 The Peruvian upwelling region

The Peruvian Upwelling Region (PUR) is one of the most productive eastern boundary upwelling regions in the world. Moderate, seasonally varying, southerly winds and associated wind stress drive upwelling of nutrient-rich Equatorial Subsurface Water (ESSW) from the subsurface Peru-Chile Undercurrent (PCUC), leading to high primary productivity in the PUR (*Brink et al.* [1983], *Penven* [2005], *Echevin et al.* [2008], *Albert et al.* [2010], *Chaigneau et al.* [2013]). Maximum winds are observed in austral winter and show a drop-off towards the coast due to land/sea surface change. Wind variations can lead to variations in upwelling intensity on time scales from 6 days to several years (*Brink et al.* [1983]).
There is equatorward flow in the mainly wind-driven Peru Coastal Current (PCC) along the Peruvian coast and poleward flow in the Peru-Chile Undercurrent (PCUC) along the outer shelf (see figure 1). *Chaigneau et al.* [2013] give a detailed description of the Northern Humboldt Current System in which the PUR lies.
Mixed-layer depths in the region are usually fairly shallow, with MLDs of less than 20m (*Brink et al.* [1983]). SST shows pronounced cycles induced by wind variations on time scales from 10 days to several years (*Brink et al.* [1983]), as well as seasonal cycle, with

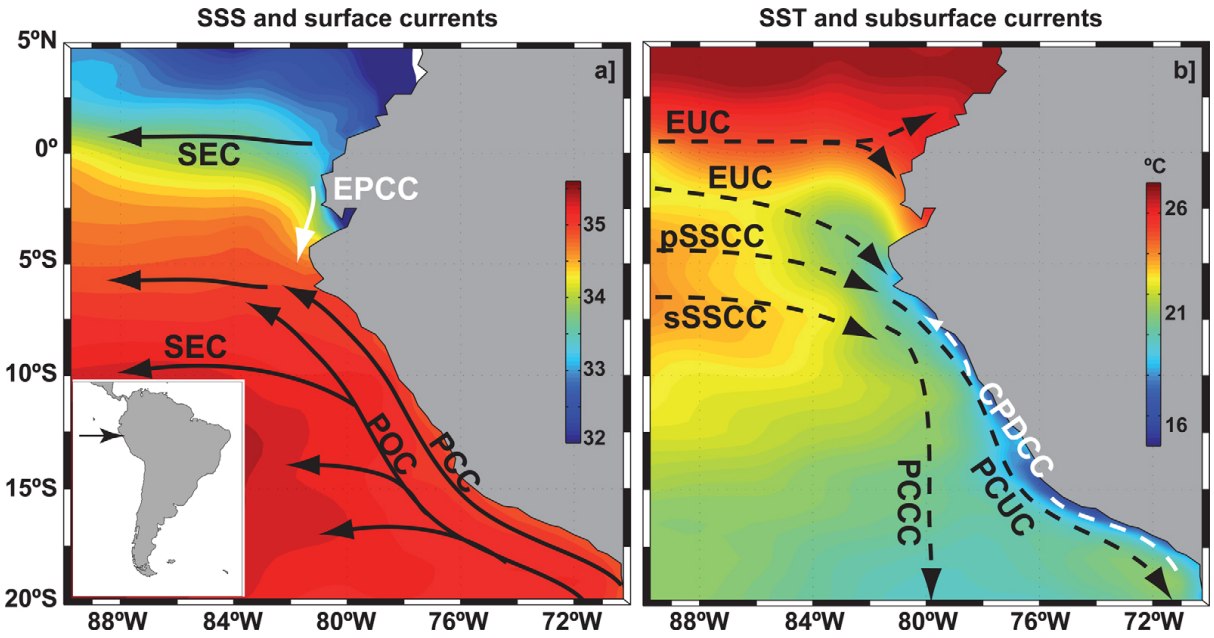

Figure 1: *(a) Surface and (b) subsurface currents of the Northern Humboldt Current System and Peruvian Upwelling Region (taken from Chaigneau et al. [2013]). Shown are (a) the Ecuador-Peru Coastal Current (EPCC), South Equatorial Current (SEC), Peru Oceanic Current (POC) and Peru Coastal Current (PCC), and (b) the Equatorial Undercurrent (EUC), primary Southern Subsurface Countercurrent (pSSCC), secondary Southern Subsurface Countercurrent (sSSCC), Peru-Chile Countercurrent (PCC), Peru-Chile Undercurrent (PCUC) and Chile-Peru Deep Coastal Current (CPDCC). Also shown are (a) sea-surface salinity (SSS) and (b) SST contours from CARS 2009 climatology data.*

maximum values of 29°C in austral summer and minimum SSTs of 14°C in austral winter (*Penven* [2005]). Coastal trapped waves have been observed in the area by *Brink et al.* [1983], with reported periods between 5-20 days. Eddy-like structures at 14°S and 17°S are a known source for generation of eddy kinetic energy and mesoscale eddies (*Chaigneau et al.* [2013]). Intraseasonal variability in wind direction and intensity and associated changes in upwelling intensity, and therefore SST gradients perpendicular to the coast, are driven by migration of the inner tropical convergence zone, ENSO events or coastal or equatorial Kelvin waves (*Dewitte et al.* [2011]).

2.3 Non-linear internal waves

The generation of non-linear internal waves is considered to be a consequence of tidal interactions with topography, such as the shelf break, and the presence of stratification in the water column (e.g *Apel and Holbrook* [1985], *Apel* [1995], *Sandstrom and Oakey* [1995], *Small et al.* [1999], *Hallock et al.* [2000], *Moum and Farmer* [2003]). Only a small part of the tidal energy (10% reported by *Pinkel et al.* [1997]) is transferred to internal tides, which have shorter wavelengths and time scales relative to the tides. Most of the energy of these internal tides goes into the formation of non-linear internal waves. This energy is then readily available for ocean mixing due to the high intensity and even shorter time scales of NLIWs (*Sandstrom and Oakey* [1995]). Non-linear internal waves can travel long distances from their generation point, life times greater than 2.5 days have been reported by *Apel and Holbrook* [1985] for experiments conducted in the Sulu sea. *Moum and Farmer* [2003] observed wave propagation speeds of $0.6ms^{-1}$ to $0.8ms^{-1}$ with amplitudes of 40m over the continental shelf off Oregon's coast, and *Pinkel et al.* [1997] reported waves traveling with more than $0.8ms^{-1}$ and amplitudes of over 60m in the western equatorial Pacific.

The velocity structure of the NLIWs, as they are propagating across the Peruvian continental shelf, can be seen in figure 2. Ahead of the wave we find downward vertical velocities, resulting in a depression of isopycnals (not shown, *Moum and Farmer* [2003]) and convergent surface flow. Waves propagating near the surface pycnocline are therefore often referred to as waves of depression (*Lamb* [2014]). A good example of this velocity structure can be seen in the intense wave event recorded around 05:00:00 UTC in figure 2. Here, vertical velocities recorded earlier show conditions before wave passage. Behind the wave, upward vertical velocities result in divergent surface flow and an elevation of isopycnals. These surface convergences and divergences can be used to track internal waves using synthetic aperture radar imaging, as described e.g. by *Jackson et al.* [2013]. Turbulence and associated mixing is created by velocity shear and shear instabilities in the wave's trough breaking along the trailing edge of the wave (*Sandstrom and Oakey* [1995],*Moum et al.* [2007]). Breaking of shoaling waves also leads to intense turbulence (e.g. *Klymak and Moum* [2003]). Non-linear internal waves were observed to transport fluid of higher or lower density in respect to surrounding waters over several kilometers and exhibit highly elevated rates of turbulent kinetic energy dissipation in trapped cores (*Lamb* [2014]). Waves with trapped cores, or, as they are often referred to, boluses, can be generated if the stratification reaches up to the sea surface or by the presence of strong shear in background currents (*Lamb* [2003]).

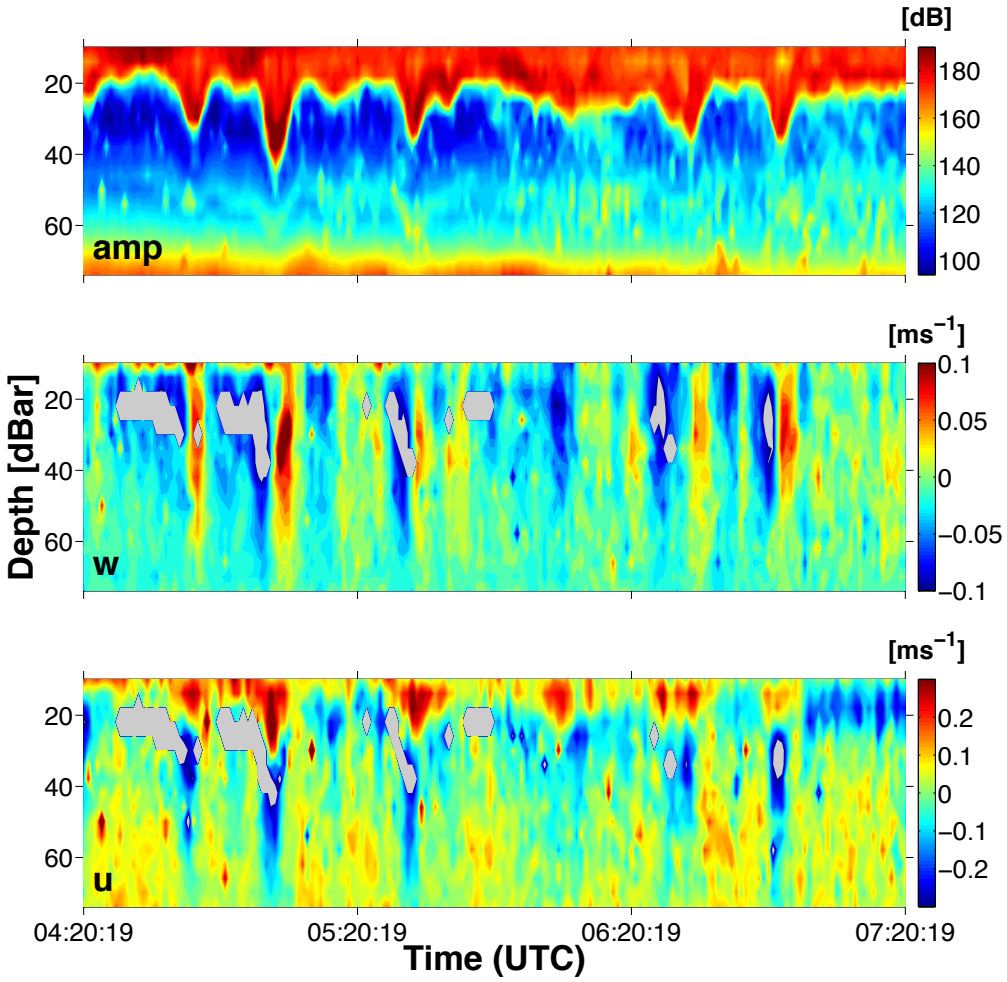

Figure 2: *(top) Backscatter amplitude, (center) vertical velocity w and (bottom) cross shore velocity u measurements of non-linear internal waves, recorded by the SLM 1 mooring on February* 8^{th}*. Grey areas correspond to missing values in the data.*

Inside such trapped cores, *Klymak and Moum* [2003], during the first measurements of their kind, observed rates of turbulent kinetic energy dissipation of $10^{-6}m^2s^{-3}$ in waves of elevation (waves propagating along the bottom). Horizontal displacement of particles ranges from 1km to tens of kilometers, as decribed by *Shroyer et al.* [2010].
Non-linear internal waves are therefore thought to play an important role not only in mixing on the continental shelf but also in the advection of nutrients and other biota and larvae.

2.4 Dissipation of turbulent kinetic energy, mixing and diapycnal heat fluxes

Diapycnal mixing, i.e. mixing across isopycnal interfaces, in the ocean is usually rather ineffective, as it requires an increase in potential energy and work done against buoyancy. Turbulence, induced e.g. through shear-instabilities by the passage of non-linear internal waves or convective processes, is a means to provide this energy. Turbulence increases diffusion of scalars such as temperature and salinity in the ocean by creating large velocity gradients on small scales between $1mm$ to $1cm$, and thus creating elevated gradients for molecular mixing to act. Elevated rates of turbulence and therefore diapycnal mixing in the region analysed in this work are thought to be the result of non-linear internal waves. A way to quantify turbulence is by calculating the rate of dissipation of turbulent kinetic energy, ε, using

$$\varepsilon = \frac{15}{2}\nu\langle\left(\frac{\partial u}{\partial z}\right)^2\rangle.$$

Here, ν is the kinematic viscosity and $\frac{\partial u}{\partial z}$ the vertical shear of horizontal velocity u. This equation is a simplification of a more complex formula, which requires the gradients of all the velocity components, u, v and w in all directions to be known, by assuming isotropic conditions (*Thorpe* [2007]). From this rate of dissipation, the turbulent eddy diffusivity for density K_ρ can be estimated, which in turn can be used to estimate diapycnal heat fluxes. It also requires the buoyancy frequency, N, to be known, which is a measure of stratification in the water column and is defined as

$$N = \sqrt{-\frac{g}{\rho}\frac{\partial \rho}{\partial z} - \frac{g^2}{c^2}},$$

where g denotes the gravitational acceleration, ρ the density of seawater and $\frac{\partial \rho}{\partial z}$ the density gradient with depth. c is the sound speed and the term $-g^2c^{-2}$ corrects for compressibility. Based on the turbulent kinetic energy equation, *Osborn* [1980] proposed the relation for the turbulent eddy diffusivity to be

$$K_\rho = \Gamma\frac{\varepsilon}{N^2},$$

with the mixing efficiency $\Gamma = \frac{R_f}{1-R_f}$. R_f denotes the flux Richardson number, a dimensionless number relating the removal of kinetic energy by buoyancy to the production of turbulent kinetic energy by velocity shear (*Thorpe* [2007]).

2.5 Hypothesis

Tidal-induced non-linear internal waves along the Peruvian continental slope and in the shelf region contribute significantly to the overall diapycnal heat flux below the mixed-layer and therefore have a great impact on the mixed-layer heat budget.
Analysis to validate this hypothesis will focus on net cooling of the mixed-layer during and after wave passage, evaluated using thermosalinograph data, and turbulent eddy diffusivity during non-linear internal wave events as well as for background conditions in the area and for the duration of the Meteor 92 cruise. An estimate of average heat fluxes as well as a relative contribution to overall diapycnal heat fluxes (inferred from wave and background conditions) below the mixed-layer will be presented.

3 Data and Methods

In this section, a short overview over the data collected during Meteor 92 and used for analysis in this work will be given. Methods employed for analysis and validation of the hypothesis will also be presented.

3.1 Data

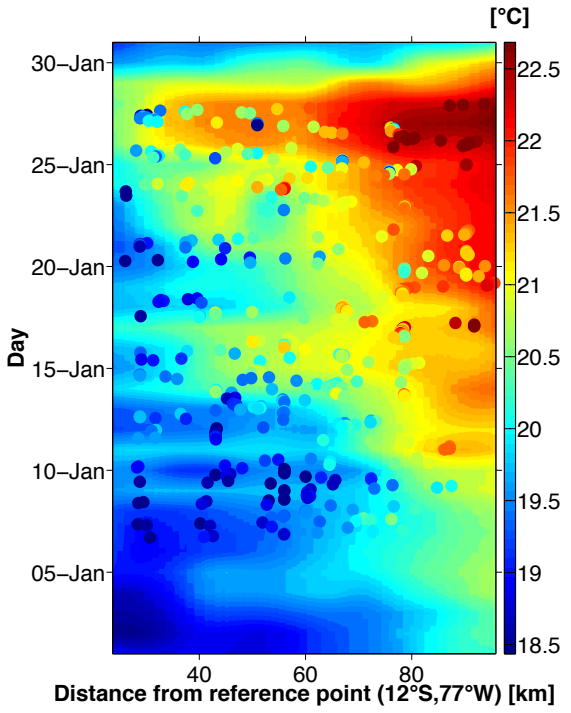

Figure 3: *MUR sea-surface temperature data (filled contours) along the repeated cross section during M92 (see also figure 4), overlayed with 60-minute mean thermosalinograph temperature data (filled dots).*

Multi-scale ultra high resolution sea-surface temperature (MUR SST) (figure 3) (downloaded from www.mur.jpl.nasa.gov/; last visited on April 12^{th} 2014) offers a spatial resolution of 1 km globally and a temporal resolution of 1 day, merging data from MODIS, AMSR-E and AVHRR products. Air-sea fluxes over the Peruvian continental slope and shelf were obtained from the Tropflux data center (www.locean-ipsl.upmc.fr/tropflux/; last visited on May 21^{st} 2014) as monthly averages from January to December 2012 with a spatial resolution of 1°. Data for 2013 was faulty and could not be used for analysis at the time of this work. Thermosalinograph data (figure 3) used for analysis of net cooling of the mixed-layer during non-linear internal wave events was analysed for the duration of M92 with a 1-minute temporal resolution, deemed high enough to resolve possible changes in temperature during NLIW events. Acoustic Doppler current profiler (ADCP) data was measured with a vessel-mounted 75kHz ADCP (VADCP) with a vertical resolution of 8m for most of M92. A vertical resolution of 4m was used for two periods, from January 16^{th}, 07:17 UTC until January 19^{th}, 00:55 UTC and from January 27^{th}, 03:24 UTC until January 28^{th}, 02:59 UTC. Temporal resolutions in both cases were 1 minute. Addtionally, ADCP data from the SLM 1 mooring (see figure 4) deployed at 80m water depth and measuring at a frequency of 300kHz from January 8^{th}, 12:00 UTC until March 3^{rd}, 18:35 UTC, was analysed.

Microstructure (MSS) profiles used for analysis of non-linear internal wave events and calculation of diapycnal heat fluxes below the mixed-layer were collected during M92 over the continental slope and in the shelf region off Peru (see also figure 4). 254 MSS profiles were measured over the course of 20 days, from January 11^{th} until January 31^{st} 2013. Profiles were not taken to specifically sample NLIW events, as done previously by e.g. *Moum et al.* [2007] and *Shroyer et al.* [2010]. Rather a broad spectrum of dissipation rates, including times, when no NLIWs were present, was targeted.

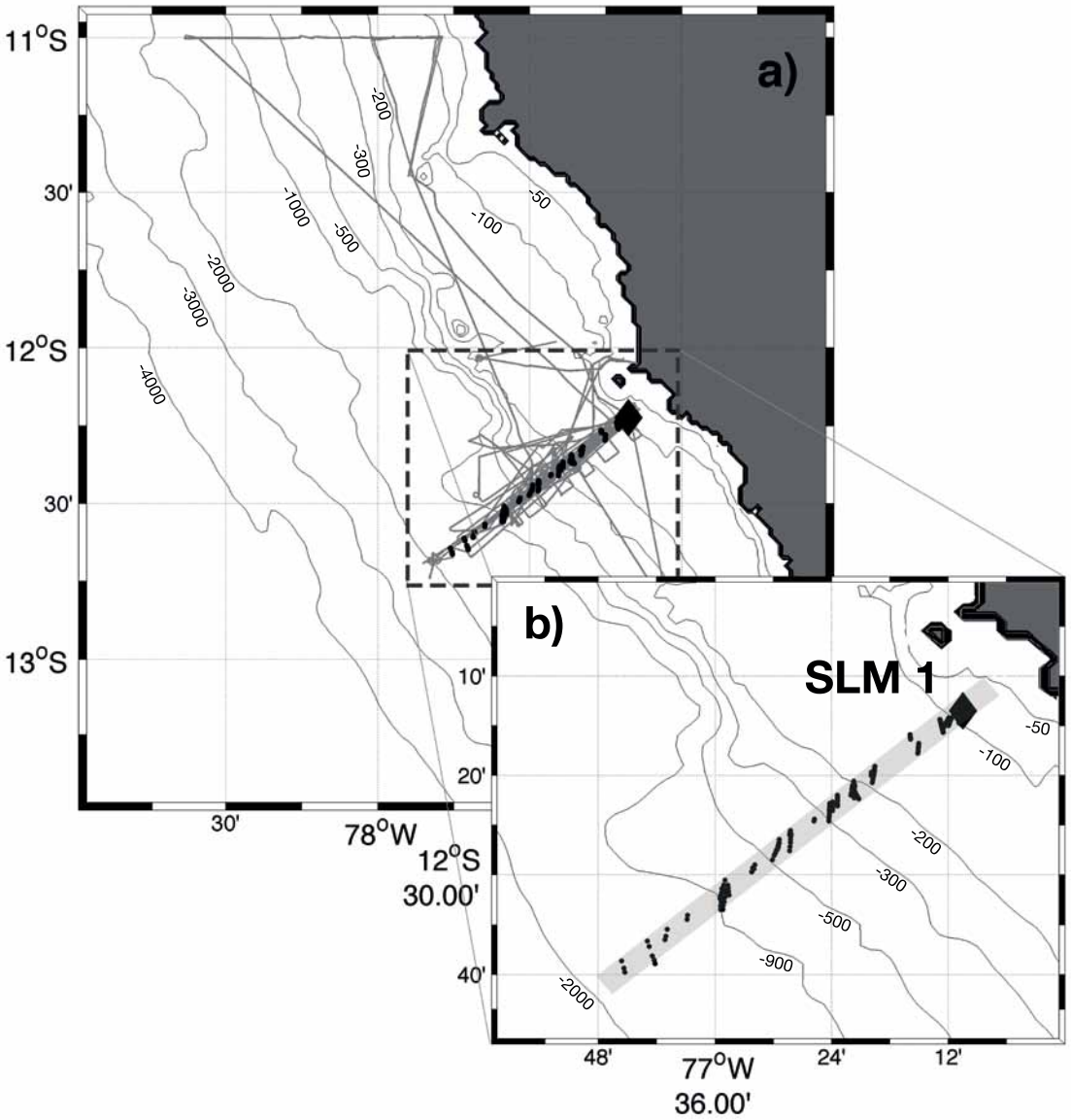

Figure 4: *(a) Cruise track of Meteor 92 (grey line) as well as positions of the SLM 1 mooring (diamond) and individual microstructure stations (dots). (b) A close up of the squared area in (a), again showing individual microstructure station and SLM 1 mooring positions. The repeated cross-section across the continental slope and shelf is shown as a shaded, light grey bar.*

3.2 Methods

For analysis of wave events through acoustic backscatter and thermosalinograh data, waves of all magnitudes were considered. This was done to cover a broad spectrum of non-linear internal waves for a more representative mean net cooling rate. Acoustic backscatter amplitudes recorded by the ships's VADCP along the cruise track were used to detect NLIW events, as done by e.g. *Moum and Farmer* [2003] or *Shroyer et al.* [2010]. Multiple wave events were analysed for duration and, using the thermosalinograph temperature just before and right after the event, to determine whether a net cooling of the mixed-layer by the NLIW had occured.

Rates of dissipation of turbulent kinetic energy (TKE) ε were estimated from airfoil probe velocity shear measurements. Measuring at a frequency of 1024Hz and averaging over 1 second intervals at a falling speed of approximately $0.6ms^{-1}$, results in a vertical resolution of about 0.6m. Assuming isotropic conditions and using the relation

$$\varepsilon = 7.5\mu \int_{k_{min}}^{k_{max}} E_{\frac{du}{dz}}(k)dk,$$

with the dynamic viscosity of seawater μ and the shear wave number spectrum $E_{\frac{du}{dz}}(k)$, integrating over a defined wave number spectrum (see also *Gregg* [1998]), ε can be estimated[1]. Rates of turbulent kinetic energy dissipation were not calculated by the author, the profiles were already despiked and readily evaluated for analysis. The measured salinity profiles were corrected against nearby Conductivity-Temperature-Depth (CTD) profiles, as the conductivity sensor used on the microstructure profiler was malfunctioning, resulting in biased conductivity and therefore salinity profiles. This was done by first calculating the bias between each individual MSS salinity profile and its adjacent CTD salinity profile, fitting a 3^{rd}-degree polynomial structure function to the bias, to account for regions of higher variability, e.g. in the mixed layer and the thermocline, and correcting the MSS salinity profiles using the 3^{rd}-degree polynomial. Profiles of buoyancy-frequency N^2 calculated from corrected salinity and measured temperature and pressure profiles were smoothed over intervals ranging from bins of 5 to 30 N^2-values (corresponding to depth- intervals of about 3m-15m) for depths mixed-layer depth (MLD) +2m to MLD+15m, to exclude very small values resulting from low stratification inside the mixed-layer. Values for N^2 below a depth of MLD+15m were then smoothed over constant intervals of 15m.

[1]For further information on the method used here, the reader is referred to e.g. *Inall et al.* [2000], *Schafstall et al.* [2010] and *Hummels et al.* [2013].

Diapycnal heat fluxes beneath the mixed-layer were estimated using the following formula:

$$J_h = -\rho \cdot c_p \cdot \frac{\Gamma \cdot \varepsilon}{N^2} \cdot \frac{\partial T}{\partial z} \tag{1}$$

(e.g. *Hummels et al.* [2013]). Diapycnal heat fluxes out of the mixed-layer are considered positive. The mixing-efficiency Γ was assumed to be 0.2, as e.g. by *Schafstall et al.* [2010] or *Moum and Farmer* [2003] and validated through simultaneous measurements of velocity shear and temperature gradients by *Oakey* [1982] and open-ocean measurements by *Moum* [1996]. Mean rates of dissipation of turbulent kinetic energy ε and the vertical temperature gradient $\frac{\partial T}{\partial z}$ were taken from microstructure measurements. Intervals were defined from just below mixed-layer to insure exclusion of values from inside the mixed-layer, as they were likely affected by wind- and surface wave-induced turbulence, to a depth of MLD+10m. Additionally, values for ε recorded at depths above 5m below the sea surface were discarded, as they are likely to have been contaminated by ship-induced turbulence. Constant specific heat capacity c_p and densitiy for seawater ρ were assumed. Mixed-layer depths were calculted from microstructure temperature profiles for each indvidual MSS profile, using the 0.2°C-criterion.

Values of $\varepsilon \geq 10^{-5}\ m^2 s^{-3}$ were scaled down by a factor of three, as they were likely overestimated due to seemingly slower falling speeds recorded by the sensor during isopycnal displacement during non-linear internal wave events (ε is strongly dependent on the falling speed, with $\varepsilon \sim w^{-4}$ (see *Inall et al.* [2000])). They may otherwise have produced unrealistically high estimates of J_h. Noise levels of ε from microstructure profilers between $1 \times 10^{-9}\ m^2 s^{-3}$ and $4 \times 10^{-10}\ m^2 s^{-3}$ were reported by *Schafstall et al.* [2010] and $10^{-10}\ m^2 s^{-3}$ by *Gregg* [1999].

To assess the impact of non-linear internal waves on the mixed-layer heat budget, the heat flux that was available for heating the mixed-layer denoted the adjusted net surface heat flux Q_{adj} after *Wang and McPhaden* [1999], was calculated using

$$Q_{adj} = Q_0 + Q_{pen}.$$

Here Q_0 is the net air-sea heat flux, and Q_{pen} describes the heat loss due to absorption of penetrating shortwave radiation in the mixed-layer. Q_{pen} is dependant on the mixed-layer depth MLD and can be calculated using

$$Q_{pen} = -0.45 \cdot Q_{sho} \cdot e^{-\gamma \cdot MLD}$$

according to *Wang and McPhaden* [1999], with Q_{sho} being the net surface shortwave radiation.

γ was assumed to be 0.04, as described by *Wang and McPhaden* [1999] and used by *Foltz et al.* [2003]. To quantify heat fluxes induced by non-linear internal waves and compare them to background conditions, profiles of turbulent kinetic energy dissipation were averaged for two cases. 16 profiles, all of them taken during wave passage, were averaged for mean dissipation rates ε_w as well as buoyancy-frequency N_w^2 and heat fluxes below the mixed-layer J_h^w for depths MLD to MLD+40m. This provided values for mean heat fluxes beneath the mixed-layer (see e.g. *Shroyer et al.* [2010]). Heat fluxes were then averaged again, for overall diapycnal heat fluxes below the mixed-layer. To compare the mean heat flux and net cooling during NLIW events to background conditions, 25 profiles during which no waves were observed were analysed as well, with values denoted here ε_b, N_b^2 and J_h^b. Additionally, depth profiles for means of ε, K_ρ and J_h as well as 95% confidence intervals from bootstrap during wave and background conditions were computed for depths MLD to MLD+40 in 10m intervals. Means for specific depth intervals will be denoted as e.g. $\varepsilon_{b(10-20)}$ from here on.

To quantify the overall impact and the cooling effect of non-linear internal waves on the mixed-layer, a time-weighted average heat flux J_h^t was calculated using

$$J_h^t = P^w \cdot J_h^w + (1 - P^w) \cdot J_h^b$$

and compared to adjusted net surface heat fluxes. Here P^w denotes the time-fraction NLIWs were present, derived from vertical velocity measurements at the SLM 1 mooring (figure 4), previously described by *Shroyer et al.* [2010]. The criterion for identifying NLIW events here was $w^2 \geq 6.25 \times 10^{-4} m^2 s^{-2}$ at a depth of 30m.

The relative contribution of NLIWs to the total heat flux was calculated using

$$\%J_h^w = \frac{P^w \cdot J_h^w}{J_h^t} \times 100.$$

4 Results

The results of this work will be presented here. Observed net cooling of the mixed-layer by non-linear internal waves will be followed by a description of wave and background conditions. Further on, a time-weighted average diapycnal heat flux and its impact on the adjusted net surface heat flux will be presented.

4.1 Observed cooling of the mixed-layer from thermosalinograph measurements

Observed net cooling of the mixed-layer by non-linear internal waves ranged from -0.001°C down to -0.14°C. 42 of these events were analysed (figures 5 and 7). They were observed using acoustic backscatter from VADCP measurements along the repeated cross-section at water depths between 80m and 1100m (figure 4). The spatial distribution, as seen in figure 5 and figure 7, shows no distinct 'hot spots', neither for observations of these events nor for their intensity. Furthermore, intensities of observed net cooling rates are fairly well distributed. However, magnitudes of single cooling events seem to be greater at deeper water depths, but the majority of the cooling events remains above -0.06°C (figure 7). The three strongest cooling events, with observed net cooling of the mixed-layer below -0.1°C, were recorded at water depths of 1100m, 850m and 250m. Events with lowest intensity, exhibiting net cooling around -0.001°C to -0.0065°C, were observed at depths 80m and 1100m, respectively. Durations of wave events ranged from 5 minutes, for less intense non-linear

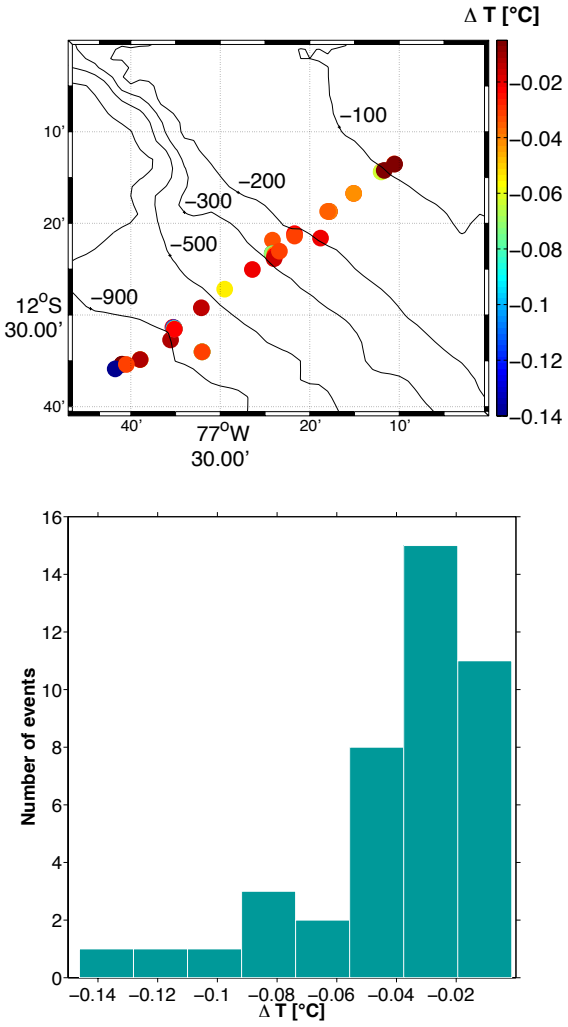

Figure 5: *(top) Locations of 42 analysed NLIW events with observed net cooling. (bottom) Histogram of temperature differences (net cooling) observed during analysed NLIW events.*

internal waves, to 12 minutes, for waves of higher magnitude. Maximum temperature anomalies in TSG data, ranging from -0.4°C to almost -3.0°C, were observed just after wave passage. Figure 6 shows non-linear internal waves as captured by VADCP acoustic backscatter as well as observed temperature anomalies, stretched to a uniform duration of 12 minutes. Analysis of all 42 cooling events revealed a mean temperature difference (net cooling of the mixed-layer) of -0.038°C after wave passage.

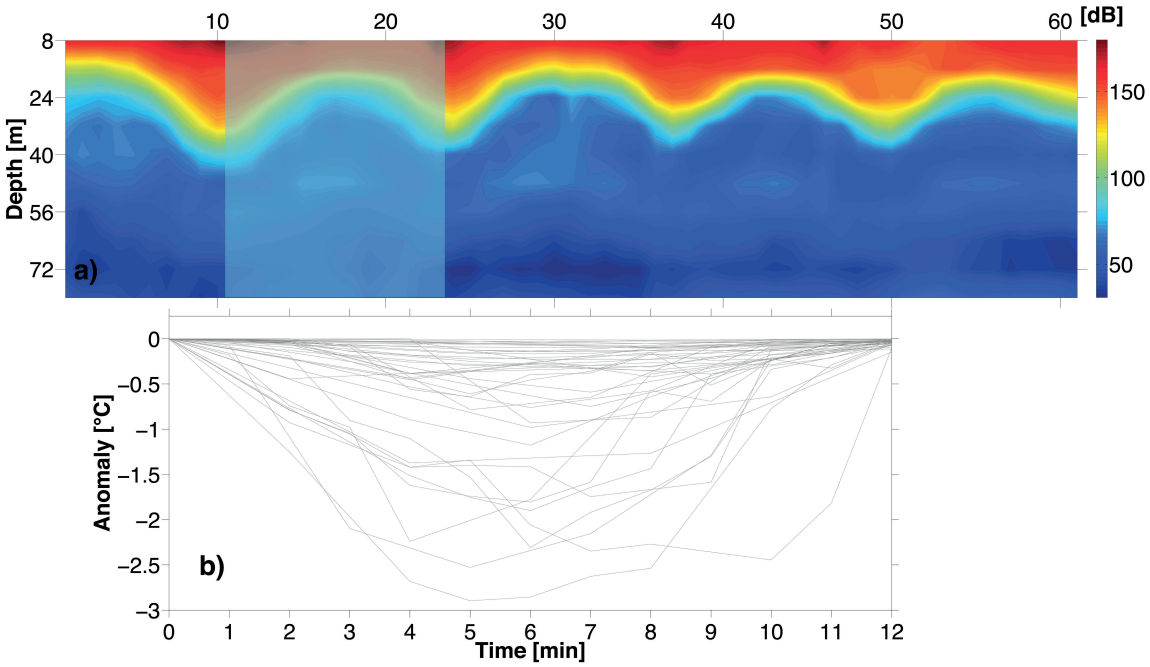

Figure 6: *(a) Examples of non-linear internal waves as captured by VADCP acoustic backscatter. (b) Temperature anomalies during non-linear internal wave events as observed and recorded using thermosalinograph measurements. Shown schematically for the shaded area in (a), data is stretched to a uniform time scale of 12 minutes for better comparison between individual events.*

4.2 Wave and background conditions

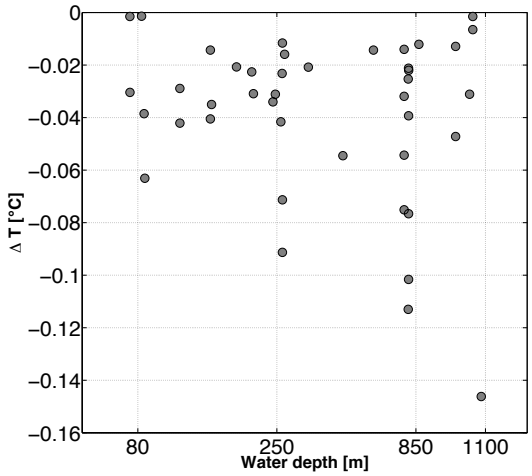

Figure 7: *Net cooling for non-linear wave events events plotted against water depth.*

In this section, observations and measurements made during wave and background conditions will first be described individually. Then a closer look at turbulent kinetic energy dissipation, turbulent eddy diffusivity and associated heat fluxes in the upper 10m below mixed-layer depth for the two mean states will be presented in a direct comparison later on.

4.2.1 Wave conditions

Figure 8 shows vertical profiles of ε_w and N_w^2 from just below the mixed layer to a depth of MLD+40m as well as temperature gradients for depths MLD to MLD+10m and locations of the 16 analysed microstructure measurements, during which non-linear internal waves were observed.

Rates of TKE dissipation in the water column below the mixed-layer, recorded during NLIW events, were highly elevated. Individual profiles showed different behavior with depth. For some, the drop-off in dissipation rates happened earlier, or at shallower depths, than for others, although it was apparent that all of them exhibited elevated rates in the upper 10m below the mixed-layer. Highest mean rates for individual profiles measured in the upper 10m below MLD were around $9 \times 10^{-6} m^2 s^{-3}$. Lowest rates recorded in this layer were $3 \times 10^{-7} m^2 s^{-3}$ and $7 \times 10^{-7} m^2 s^{-3}$. The mean dissipation rate $\varepsilon_{w(0-10)}$ in the upper 10m below MLD was $3.40 \times 10^{-6} m^2 s^{-3}$, changing only slightly with depth, as seen in figures 8a and 9a. Elevated mean dissipation rates around $2 \times 10^{-6} m^2 s^{-3}$ and $9 \times 10^{-7} m^2 s^{-3}$ could still be found at depths MLD+10m to MLD+20m and MLD+20m to MLD+30m, respectively. From MLD+30m on, mean dissipation rates went below $10^{-6} m^2 s^{-3}$ (figure 8a) and down to $6 \times 10^{-8} m^2 s^{-3}$ at MLD+30m to MLD+40m (figure 9a).

Buoyancy frequency N_w^2 showed highest levels in the upper 5m below MLD, decreasing nearly exponentially with depth (figure 8b).

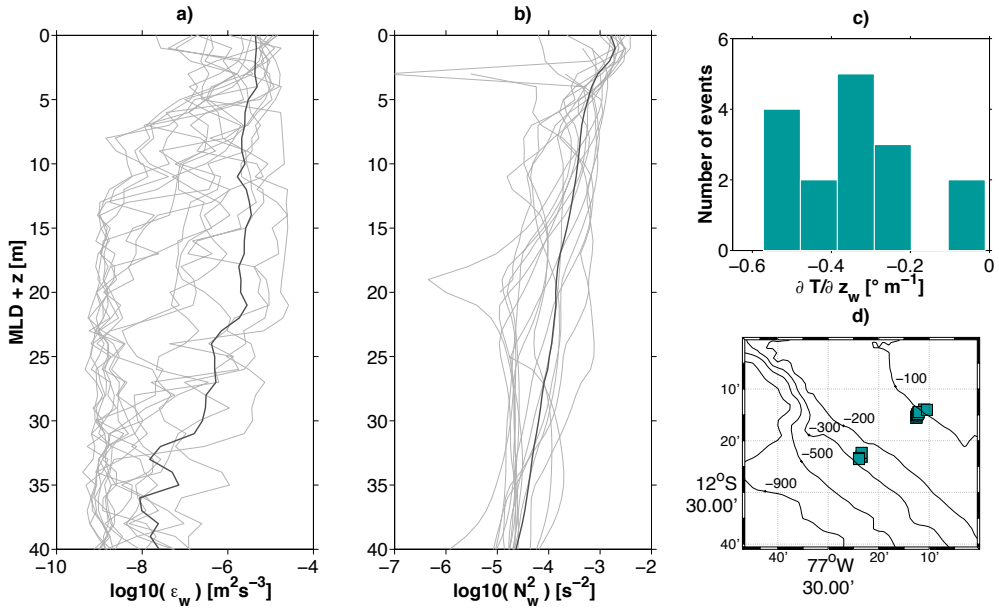

Figure 8: *(a,b) Profiles of turbulent kinetic energy dissipation ε_w and buoyancy-frequency N_w^2, recorded during NLIW events. 16 Profiles from just under the mixed-layer to a depth of MLD+40m are shown in light gray, means for the same depth interval are shown with a thick, dark gray line. (c) Histogram of vertical temperature gradients $\frac{\partial T}{\partial z}_w$ from MLD to MLD+10m for the same events. (d) Profile locations with depth contours.*

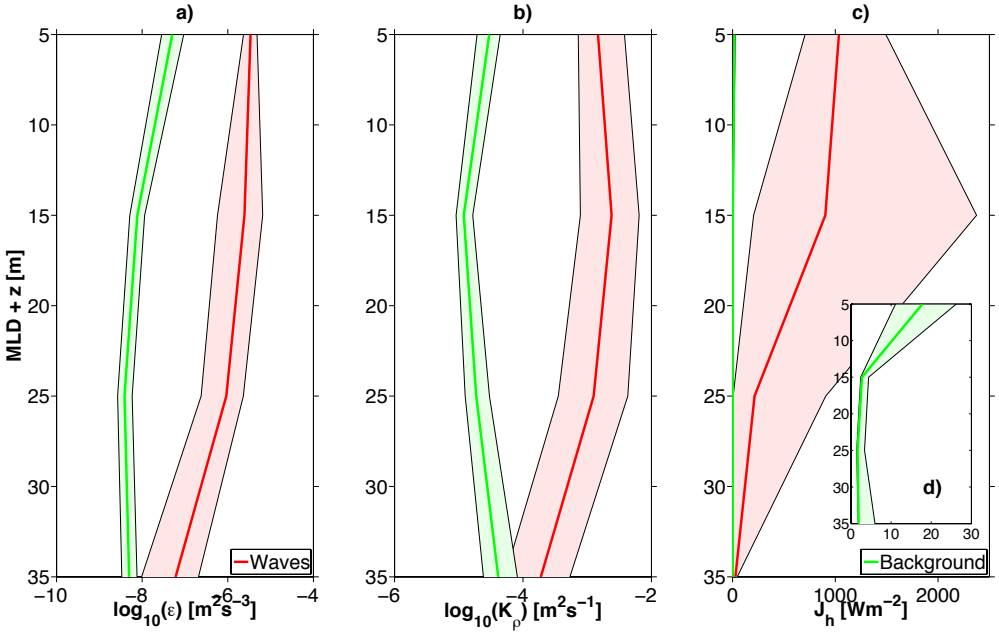

Figure 9: *Depth profiles of (a) turbulent kinetic energy dissipation ε, (b) turbulent eddy diffusivity K_ρ and (c) heat flux J_h ((d) shows a close-up of J_h^b) for depths MLD to MLD + 40m for wave (red) and background (green) conditions. Mean values are shown for 10m intervals. Shaded areas depict 95% confidence intervals from bootstrap.*

Maximum and minimum mean values were around $8 \times 10^{-4} s^{-2}$ in the upper 10m below MLD and $4 \times 10^{-5} s^{-2}$ from depths MLD+30m to MLD+40m, respectively. Spikes at depths MLD+3m and MLD+19m are remnants that did not get smoothed out.
Levels of turbulent eddy diffusivity K_ρ^w were highest between MLD+10m to MLD+20m, with a mean of $2.40 \times 10^{-3} m^2 s^{-1}$ (figure 9b), corresponding to the aforementioned only slight change in ε_w compared to the upper 10m and the decrease in N_w^2 at this depth. Values for K_ρ decreased from there on, following ε_w, to a minimum of $1.90 \times 10^{-4} m^2 s^{-1}$ between MLD+30m and MLD+40m (figure 9b).
Vertical temperature gradients in the upper layer were steep, also expected due to high turbulence during NLIW events, down to $-0.57 \frac{^\circ C}{m}$ (figure 8c). The mean gradient here was $-0.347 \frac{^\circ C}{m}$. The median gradient was $-0.349 \frac{^\circ C}{m}$, close to the mean. Temperature gradients below MLD+20m (not shown) decreased by up to two orders of magnitude. Still, stronger gradients, of the order of $10^{-1} \frac{^\circ C}{m}$, could be observed at depths between MLD+10m to MLD+30m.
Resulting mean heat fluxes J_h^w were highest in the upper 20m below MLD, with means $J_{0-10}^w = 1035 W m^{-2}$ and $J_{10-20}^w = 900 W m^{-2}$. From there on, a sharp decrease to lower, yet still elevated, values of $J_{20-30}^w = 210 W m^{-2}$ was observed, further decreasing to $J_{30-40}^w = 25 W m^{-2}$ (figure 9c). Error bounds for J_h^w from bootstrap, shown as shaded areas in figure 9c, are largest for $J_{h(10-20)}$, with $[205, 2375] W m^{-2}$. The high upper bound here is resulting from the previously mentioned odd high temperature gradients and lower stratification, i.e. higher K_ρ, at this depth. Error bounds in the layer above are $[705, 1490] W m^{-2}$.

Occurrences of NLIW events, as observed during microstructure measurements and seen in figure 8d, appear to have been most frequent at depths between 80m-120m and 250m-300m. This distribution suggests a comparison of measured rates of turbulent kinetic energy dissipation, turbulent eddy diffusivity as well as calculated heat fluxes at these water depths.

	$\varepsilon_w [m^2 s^{-3}]$		$K_\rho^w [m^2 s^{-1}]$		$J_h^w [W m^{-2}]$	
MLD + z [m]	80m	250m	80m	250m	80m	250m
0 to 10	2.9×10^{-6}	5.0×10^{-6}	7.2×10^{-4}	3.7×10^{-3}	975	1220
10 to 20	5.9×10^{-7}	8.0×10^{-6}	2.2×10^{-3}	2.9×10^{-3}	210	2990
20 to 30	3.8×10^{-7}	2.6×10^{-6}	1.0×10^{-3}	1.9×10^{-3}	3	950
30 to 40	5.3×10^{-8}	8.3×10^{-8}	1.0×10^{-4}	4.5×10^{-4}	30	22

Table 1: *Mean values of ε_w, K_ρ^w and J_h^w below the mixed-layer for 10m intervals at water depths 80m and 250 m.*

Mean values for ε_w,K_ρ^w and J_h^w for 10m depth intervals at the respective water depths of 80m and 250m are shown in table 1.

Dissipation rates at 80m depth were decreasing steadily with depth. Maximum mean values recorded here were $2.9 \times 10^{-6} m^2 s^{-3}$, decreasing by about two orders of magnitude to $5.3 \times 10^{-8} m^2 s^{-3}$ over three depth intervals. Values of turbulent eddy diffusivity were largest between depths MLD+10m to MLD+30m. Resulting heat fluxes were highest in the layer directly beneath the mixed-layer, with $J_{h(0-10)}^{80} = 975 W m^{-2}$. Minimum mean heat fluxes at this water depth were observed between MLD+20m and MLD+30m.

At 250m water depth, maximum rates of TKE dissipation were recorded deeper in the water column, from MLD+10m to MLD+20m, compared to rates at 80m. Overall, values for ε_w^{250} were higher than for ε_w^{80} and exhibited a steeper vertical gradient (table 1). K_ρ^{250} exhibited similar behavior with depth as ε_w^{80}, decreasing from a maximum mean value of $3.7 \times 10^{-3} m^2 s^{-1}$ in the upper layer below MLD to a minimum of $4.5 \times 10^{-4} m^2 s^{-1}$ recorded between MLD+30m to MLD+40m. High mean heat fluxes, associated with the behavior of ε_w^{250} with depth in these intervals, of $J_{h(0-10)}^{250} = 1220 W m^{-2}$ and $J_{h(10-20)}^{250} = 2990 W m^{-2}$ were observed, together with a sharp decrease to still highly elevated values between MLD+20 and MLD+30 and a minimum of $22 W m^{-2}$ in the lowest interval beneath the mixed-layer (table 1).

4.2.2 Background conditions

Dissipation rates for background conditions seen in figure 10 were significantly lower than during NLIW events, on average two orders of magnitude. Lowest rates of the order of $10^{-9} m^2 s^{-3}$, close to noise level, were recorded in every interval from MLD to MLD+40m. Although NLIWs were not observed while background profiles were recorded, some profiles in the upper 10m below MLD still exhibited elevated rates of TKE dissipation above $1 \times 10^{-7} m^2 s^{-3}$, resulting in a slightly elevated mean ε_b in that layer. Therefore, means range from $\varepsilon_{0-10}^b = 5 \times 10^{-8} m^2 s^{-3}$ to $\varepsilon_{30-40}^b = 5 \times 10^{-9} m^2 s^{-3}$ (figure 9a). Minimum mean dissipation rates are found at depth MLD+25m (figure 10a). At depths between MLD+25m and MLD+35m, ever so slightly elevated dissipation rates were observed (figure 10a), again leading to a higher mean ε_b between MLD+30m and MLD+40m (figure 9a).

Overall, values of N_b^2 were lower than during wave conditions, decreasing from a mean of $3.4 \times 10^{-4} s^{-2}$ in the upper 10m below MLD to $3.2 \times 10^{-5} s^{-2}$ at MLD+30 to MLD+40 (figure 10b). Also, the behavior of N_b^2 with depth compared to wave conditions was smoother, with no strongly pronounced peaks.

Resulting values for K_ρ^b were lowest between MLD+10m and MLD+20m (figure 9b).

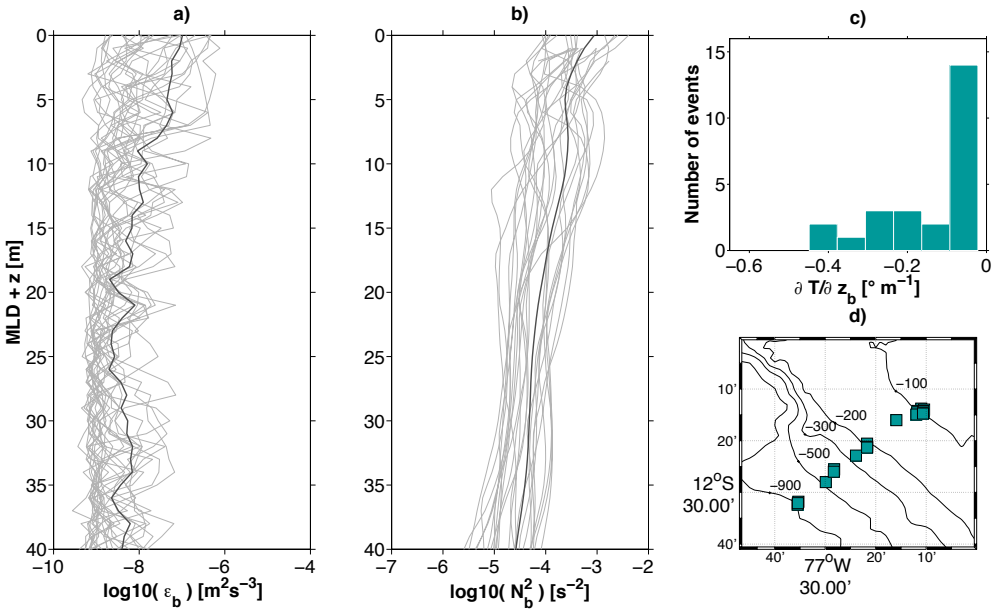

Figure 10: *Same as fig.8, but for background conditions* ε_b, N_b^2 *and* $\frac{\partial T}{\partial z}_b$ *from 25 profiles, when no NLIW events occurred.*

Mean values for K_ρ between MLD to MLD+10m and MLD+30 to MLD+40m were around $5 \times 10^{-5} m^2 s^{-1}$. Compared to wave conditions, the mean temperature gradient from MLD to MLD+10m was smaller (figure 10c) by roughly a factor of 2.5. The mean and median vertical temperature gradient $\frac{\partial T}{\partial z}_{b(0-10)}$ during background conditions was $-0.146 \frac{^\circ C}{m}$ and $-0.061 \frac{^\circ C}{m}$, respectively.

Observed diapycnal heat fluxes below the mixed-layer during background conditions were small. The mean heat flux in the upper 10m below MLD was $17 W m^{-2}$, with error bounds $[11, 26] W m^{-2}$. Below that, a sharp decrease to $J^b_{h(10-20)} = 3 W m^{-2}$ and $J^b_{h(20-30)} = 1.5 W m^{-2}$ is followed by a slight increase to $J^b_{h(30-40)} = 2 W m^{-2}$, with error bounds $[1.5, 6] W m^{-2}$, resulting from the aforementioned enhanced $\varepsilon_{b(30-40)}$ (figure 9).

As these 25 profiles were evaluated to depict typical background conditions in the area, their locations, as seen in figure 10d, are spread out over the entire cross section. Still, local differences in background heat flux intensity were observed, as shown in table 2. Maximum mean background heat fluxes at water depths around 500m were higher by almost a factor of 10 compared to fluxes at water depths 100m and 250m.

Water depth	100m	250m	500m	900m
$J^b_h [W m^{-2}]$	8	9.5	72	24.5

Table 2: *Mean heat fluxes* J^b_h *in the upper 10m below the mixed-layer at water depths 100m, 250m, 500m and 900m, as observed during background conditions. See also figure 10d for profile locations.*

4.2.3 Comparison of wave and background conditions in the upper 10m below mixed-layer depth

Since observed mean heat fluxes and rates of turbulent kinetic energy dissipation were highest in the layer directly below the mixed-layer, and it therefore seems to play an important role in the effect of non-linear internal waves on the mixed-layer heat budget, this section will present a closer look at individual profile means of ε, K_ρ and J_h for background and wave conditions in this layer. Figure 11 shows distributions and occurrences

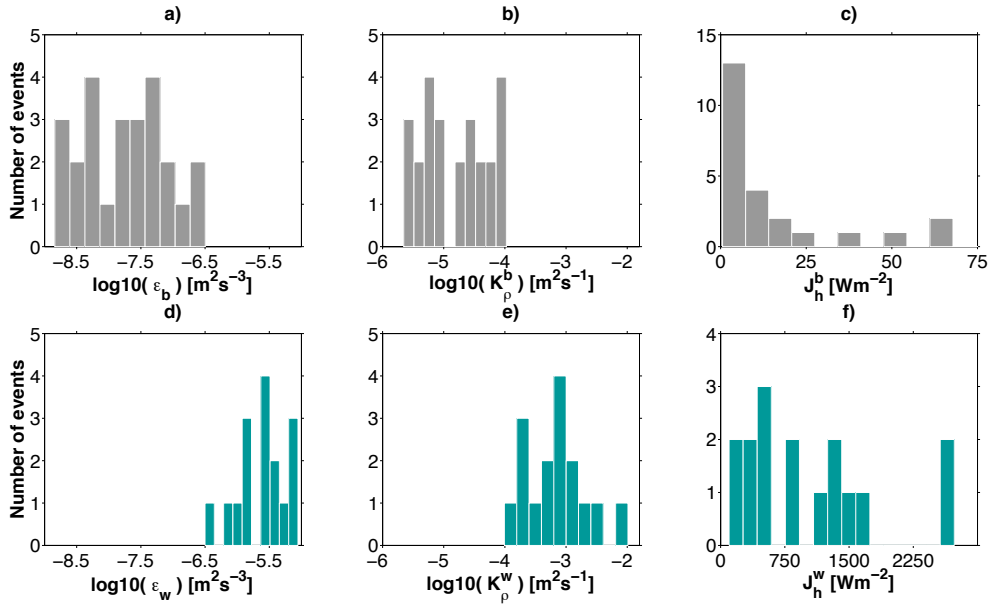

Figure 11: *Histograms of (a,d) turbulent kinetic energy dissipation ε, (b,e) turbulent eddy diffusivity K_ρ and (c,f) diapycnal heat fluxes J_h below the the mixed-layer for background conditions (top) and during NLIW events (bottom). (Note, that x-axes in c) and f) do not show the same limits.)*

of mean values for ε, K_ρ and J_h for individual profiles in the upper 10m below MLD during wave (bottom) and background (top) conditions. Corresponding axes show the same limits, except for figure 11 c and f.

Recorded values for ε_b range over two orders of magnitude, whereas ε_w ranges over a little less than 1.5 orders of magnitude, indicating a higher variance for profiles recorded during background conditions. The upper limit for ε_b, as seen in figure 11a, was $3.2 \times 10^{-7} m^2 s^{-3}$, which, evidently, was the lower limit for ε_w measured during wave conditions and can be seen in figure 11d. The same differentiation can be seen in figure 11 b and e, for values of K_ρ^b and K_ρ^w. Here, the respective upper and lower limit was of the order of $10^{-4} m^2 s^{-1}$. The median value for K_ρ^b was $1.6 \times 10^{-5} m^2 s^{-1}$, close to the mean and values ranging over more than 1.5 orders of magnitude. Values for K_ρ^w were distributed almost symmetrical,

with a slight inclination towards lower values, the median value here being $7 \times 10^{-4} m^2 s^{-1}$. Individual profiles during wave and background conditions differed by almost four orders of magnitude.

Diapycnal heat fluxes calculated from individual profiles during background conditions were mostly small, with a median value of $6 W m^{-2}$, around a third of the mean (see section 4.2.2). Although isolated, larger heat fluxes were also observed (see also table 2). Values for J_h^w showed larger variance and the median value here was $850 W m^{-2}$, roughly of the same order as the mean. Two events of intense heat fluxes $J_h^w > 2000 W m^{-2}$ were observed.

4.3 Time-weighted average diapycnal heat flux and net surface heat fluxes

Analysis of vertical velocities from the SLM 1 mooring (figures 2 and 4) revealed that non-linear internal waves were present for about a fraction of $P^w = 0.07$ of the time.

Using mean values for $J^w_{h(0-10)}$ and $J^b_{h(0-10)}$ described in sections 4.2.1 and 4.2.2, this estimate leads to a time-weighted average diapycnal heat flux of $J^t_{h(0-10)} = 90 W m^{-2}$ directly below the mixed-layer. Based on 95% error bounds for $J^w_{h(0-10)}$ (figure 9), non-linear internal waves contributed between 75% and 85% of the total diapycnal heat flux directly below the mixed-layer.

Figure 12 shows monthly mean values for net surface shortwave radiation and net surface heat flux over the continental shelf and in the area of Meteor 92 for the year 2012. Additionally, the heat loss of shortwave radiation penetrating the mixed-layer and the resulting adjusted net surface heat flux are shown, calculated for a mean mixed-layer depth of 10m. We see a seasonal cycle in net surface shortwave radiation with minimum and maximum values of $125 W m^{-2}$ and $250 W m^{-2}$, observed during austral winter and austral summer, respectively. Net surface heat fluxes show a similar, but more pronounced cycle, with minimum and maximum values of $-20 W m^{-2}$ and $150 W m^{-2}$, respectively. The mean mixed-layer depth observed during M92 and hence resutling values for adjusted net surface heat fluxes over the continental shelf are fairly representative for summer and autumn in the area of M92, but less so for winter and spring. Mean net air-sea heat fluxes of $150 W m^{-2}$ (from Tropflux data) in January led to an adjusted net surface heat flux of $80 W m^{-2}$ (figure 12), meaning that diapycnal heat fluxes beneath the mixed-layer transported more than 100% of that heat away from the mixed-layer.

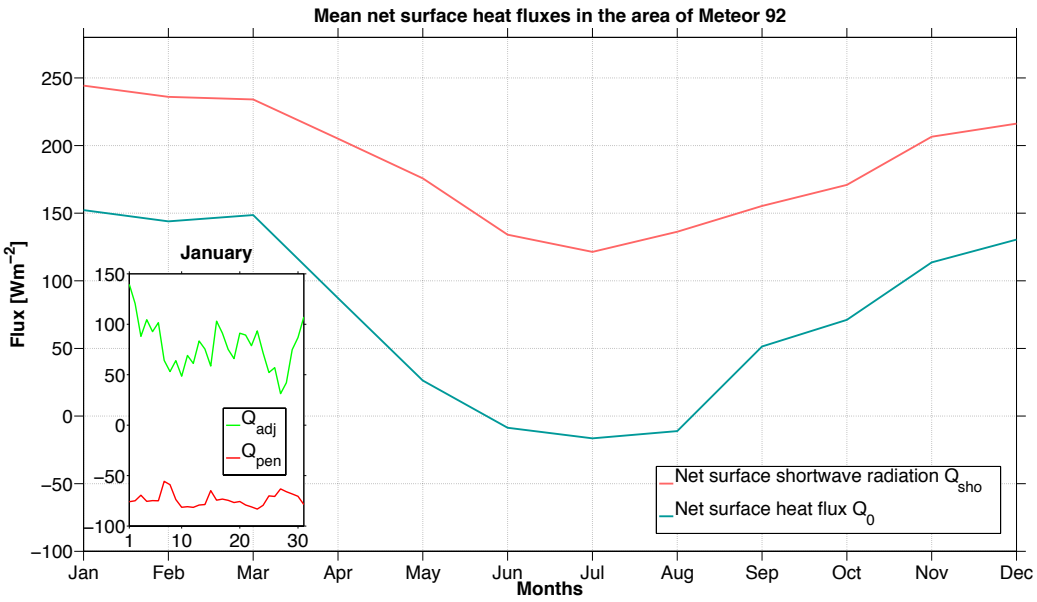

Figure 12: *Monthly mean values for net surface shortwave radiation (blue), net surface heat flux (yellow). Means are shown for 2012 in the area of Meteor 92. Adjusted net surface heat flux (green) and heat loss of shortwave radiation penetrating the mixed-layer (red) are shown for January, calculated assuming a mean mixed-layer depth of 10m.*

Based on the mean values for $J^{80}_{h(0-10)}$ and $J^{250}_{h(0-10)}$ presented at the end of section 4.2.1, non-linear internal waves supplied around 81% of the diapycnal heat flux at 80m water depth, compared to 84% at 250m depth. The difference in relative contributions at the two depths is more pronounced in layers beneath MLD+10m, as highest diapycnal heat fluxes at 250m water depth were observed here (see section 4.2.1 and table 1) and background heat fluxes were small. Between MLD+10m to MLD+20m, non-linear internal waves accounted for 98% of the overall diapycnal heat flux at 250m compared to 84% at 80m water depth. At MLD+20m to MLD+30m they contributed 97% and 13%, respectively. Between MLD+30m to MLD+40m, with diapycnal heat fluxes at 250m sharply decreasing and a small increase at 80m water depth, contributions were about the same, at 40%.

5 Discussion

The discussion will be divided into four parts. First, the results of this work will be summarized. Then, said results will be discussed and compared to previous studies. Eventually, a discussion of possible errors will be followed by an outlook on future opportunities and suggestions for improvements on the methods presented here.

5.1 Summary

Main objective of this work was to quantify diapycnal heat fluxes below the mixed-layer induced by non-linear internal waves along the continental slope and shelf region off Peru. Microstructure measurements, acoustic backscatter and thermosalinograph data, all collected during the Meteor 92 research cruise in January 2013, were analysed and led to the following results:

- On average, non-linear wave events, as observed with VADCP acoustic backscatter and analysed using thermosalinograph data, led to local net cooling of the mixed-layer of -0.038°C after wave passage. Distinct regions over the continental slope and shelf with particularly high or low net cooling events could not be identified within the 42 analysed wave events.
- Compared to background conditions, rates of turbulent kinetic energy dissipation, recorded while non-linear internal waves were present, were highly elevated, by about two orders of magnitude. Rates exceeding $10^{-5} m^2 s^{-3}$ were observed below the mixed-layer.
- Resulting mean diapycnal heat fluxes below the mixed-layer during wave conditions were about 60 times higher than during background conditions.
- A comparison of profiles taken at water depths of 80m and 250m showed that heat fluxes induced by non-linear internal waves observed at larger water depths were overall higher and showed a larger vertical extend, exhibiting heat fluxes of almost $3000 W m^{-2}$ between 10m to 20m below mixed-layer depth.
- Background heat fluxes below the mixed-layer showed intensifications at water depths around 500m. Values for J_h^b observed here were almost 10 times higher than at depths 100m and 250m and 3 times higher than at 900m.

- Analysis of vertical velocities from SLM 1 mooring data, taken at 12°13.51" S, 77°10.5" W at 80m water depth, reveiled that non-linear internal waves were present on the shelf for a fraction of 0.07 of the time.
- In a time-weighted sense, non-linear internal waves supplied between 75% to 85% of the total diapycnal heat flux below the mixed-layer. Spatial variations in relative contributions between different water depths were observed.
- The total diapycnal heat flux in the layer directly below the mixed-layer, as inferred from background and wave conditions, was $90 W m^{-2}$, compensating for more than 100% of the adjusted net air-sea heat flux on the continental shelf.

5.2 Discussion of results

Using analyses described in this work, it could be shown that non-linear internal waves, through their induced turbulence and diapycnal heat fluxes below the mixed-layer, have a major impact on the mixed-layer heat budget on the Peruvian shelf. In this section, a comparison of the results presented in this work with other studies and a general discussion will be presented.

Results from thermosalinograph measurements for net cooling of the mixed-layer induced by individual non-linear internal waves were slightly higher compared to results reported by *Shroyer et al.* [2010], who concluded non-linear internal waves leading to a net cooling of the mixed-layer of 0.1°C per day. They inferred their cooling rates from heat-flux divergences at the pycnocline. Since wave events were handpicked and identification was sometimes difficult, especially in cases when multiple waves inside a wave packet were appearing in short intervals closely together, the observed temperature differences between moments before and after the event might differ from real values. The majority of the analysed events was observed during times when the ship was standing or only moving very slowly, with ship speeds below 1kn. In cases when the ship was going at cruising speed, wave events were often only captured very distorted, if captured at all, and generally could not be considered for analysis. The distribution of maximum cooling rates and the magnitude of cooling events observed at greater water depths coincides with the results obtained from heat flux calculations. Wave events observed seaward from the shelf break could be reflected waves (*Munk* [1981]) or waves generated at the shelf break and moving seaward (*Henyey and Hoering* [1997]).

Background heat fluxes estimated for water depths around 500m were close to the estimate made by *Shroyer et al.* [2010]. During their study in the northern west Atlantic

they specifically sampled conditions before non-linear internal wave passage, which they had identified previously through high frequency echosounder, to compare them to wave conditions. Their estimate of average background heat fluxes over New Jersey's continental shelf came to $80 W m^{-2}$. Overall background heat fluxes in the upper 10m below the mixed-layer presented in this work were about four times smaller than those reported by *Shroyer et al.* [2010]. The elevated rates of dissipation and resulting enhanced diapycnal heat fluxes observed at water depths greater than 500m could result from inertia gravity waves.

Heat fluxes during wave conditions were roughly of the same order as means described by *Shroyer et al.* [2010]. Individual strong mixing events in excess of $2000 W m^{-2}$, as observed here, were also reported by *Moum and Farmer* [2003] over Oregon's continental shelf. Contrary to these observations, *Inall et al.* [2000] reported across-pycnocline heat fluxes of $80 W m^{-2}$ on the Malin shelf during neap tides for a wave period of 12.4 hours. The ratio of wave to background conditions estimated here was 60:1, six times larger than the estimate made by *Shroyer et al.* [2010]. Reasons for this could be the relative undersampling of wave events. The 16 analysed profiles taken during non-linear internal wave passage might not represent typical wave conditions in the area, the few observed strong wave events, which led to diapycnal heat fluxes over $2000 W m^{-2}$, biasing the estimate for average heat fluxes. Another reason might simply be a different internal wave field in the region off Peru than off Oregon, as local topographic features on the shelf strongly influence wave generation, dissipation rates as well as their intensity and the very nature of dissipation processes that can occurr (*Lamb* [2014]).
Sandstrom and Oakey [1995] and *Sandstrom and Elliott* [2011] reported a decrease in wave energy of shoreward propagating non-linear internal waves. *Inall et al.* [2000] concluded that magnitudes of observed enhanced mixing and dissipation rates must decrease in the shoreward direction. Observations made over the Peruvian shelf and the results presented here also indicate that heat fluxes induced by non-linear internal waves near the shelf break as a result of higher dissipation rates were more intense and reaching deeper into the water column than shoreward from the shelf break.

The estimate for $P^w = 0.07$ made in section 4.3 is rather conservative, compared to previous observations, that wave packets in the area usually consist of about 7 single waves, each event with a duration of approximately 10 minutes, occurring with the semi-diurnal tides (Dengler, personal correspondence). Estimated time fractions from these observations would result in $P_e^w = 0.097$. On average, *Shroyer et al.* [2010] observed packets consisting of 10 waves, in aggreement with *Inall et al.* [2000], reporting the same number of waves in NLIW packets on the Malin shelf. The approximation of P^w is highly

dependent on the criterion set for w^2. Changing the criterion $w^2 \geq 6.25 \times 10^{-4} m^2 s^{-2}$ by only $2.5 \times 10^{-5} m^2 s^{-2}$, leads to a change in P^w of about a factor 2. Though of the same order as the average time fraction non-linear internal waves were present on the shelf off New Jersey reported by *Shroyer et al.* [2010], estimates here might be too low and therefore underestimate the imact of NLIWs in the region. At rather shallow depths, single non-linear internal waves might not be clearly distinguishable from one another due to interference and interaction of individual waves and wave packets of different generations with one another, as described by *Apel* [1995]. In agreement, *Shroyer et al.* [2010] reported smaller time fractions shoreward from the shelf break and since only the mooring at 80m water depth was taken into consideration for the calculation of P^w, time fractions might be further underestimated. As time-weighted overall diapycnal heat fluxes depend on the time fraction P^w, the estimate presented here might consequently be too low.

Hummels et al. [2013] concluded that diapycnal heat fluxes induced by turbulence are a major contributor to the mixed-layer heat budget and play a big role in cooling the mixed-layer in the Atlantic cold tongue. Though their study did not revolve around non-linear internal waves in particular and results can therefore not be directly compared, the findings of this work here also indicate a large impact of NLIW-induced diapycnal heat fluxes on the mixed-layer heat budget over the Peruvian shelf. Overall diapycnal heat fluxes, with non-linear internal waves contributing around 80% through turbulence, transported more than 100% of the adjusted net surface heat flux away from the mixed-layer, validating their high impact on the mixed-layer heat budget. This result is in agreement with *Shroyer et al.* [2010], who concluded that NLIWs transported all of the incoming heat away from the mixed-layer, basically leading to cooling by diapycnal heat fluxes at the bottom of the mixed-layer cancelling out heating by net surface heat fluxes. Although their estimated relative contribution of non-linear internal waves was lower than concluded in this study, higher overall background heat fluxes were observed, leading to higher time-weighted overall heat fluxes over the shelf off New Jersey.

Net surface shortwave radiation and net surface heat fluxes show lower values in austral winter mainly due to lower insolation and higher latent heat loss. Exact values of net surface shortwave radiation and net surface heat fluxes might not be fully representative of the conditions observed during M92, but the obvious seasonality adduced here should suffice to assess the impact of non-linear internal waves. Provided their impact remained the same throughout the year, this seasonality of net surface heat fluxes would lead to even higher compensation of adjusted net heat fluxes and therefore cooling of the mixed-layer by non-linear internal waves in fall and winter. The factor γ was reported to be

higher in productive regions (*Wang and McPhaden* [1999]) and therefore would also show a seasonal and spatial variability. The sensitivity of the adjusted net surface heat flux to changes in γ is reportedly fairly small though, according to *Wang and McPhaden* [1999]. A deeper mixed-layer in austral winter would result in higher relative adjusted net surface heat fluxes, counteracting the higher impact of non-linear internal waves.

Based on their error bounds, *Shroyer et al.* [2010] estimated non-linear internal waves to contribute between 20% to 67% to the overall heat flux below the mixed-layer. Due to these large error bounds, their conclusion, that non-linear internal waves transported all heat away from the mixed-layer, might only be the case for individual events of higher intensity or certain regions on the shelf. Error bounds for heat fluxes in this study were smaller, leading to an estimate of wave contribution of 75% to 85%. Below the upper layer beneath the mixed-layer, the ratio of heat fluxes during wave conditions compared to background conditions was different for different water depths, as heat fluxes in that layer were much higher at water depth 250m compared to 80m.

As made clear in this work, different wave and background heat flux intensities at different water depths were observed. Therefore, a spatial variability in the impact of non-linear internal waves on the mixed-layer heat budget is implied, warranting further investigation. The exact contribution of non-linear internal waves to the mixed-layer heat budget cannot be estimated at this point due to the lack of sufficient data and seasonal and spatial coverage. It is important to note that analysis performed in this study only reflects the impact of diapycnal heat fluxes on the mixed-layer heat budget. Advective processes might additionally heat or cool the mixed-layer. For a fully representative analysis, the complete mixed-layer heat budget, including lateral advection and heat storage terms, as described by *Stevenson and Niiler* [1983], need to be evaluated.

5.3 Error discussion

Errors in calculated temperature differences lie in the ability of identifying start and end points of such an event as well as the event itself. Especially when waves were following closely behind each other, the temperature recorded by thermosalinograph measurements might not have completely returned to its new steady state and therefore the calculated differences might be too high. As described before, estimated values here could be wrong by a few thousandths to a few hundredths of degrees. This error would be significant, as observed temperature differences were of the same order.
Overestimation of K_ρ by applying the Osborn model, as described by *Barry et al.* [2001], *Shih et al.* [2005] and *Ivey et al.* [2008], could lead to an overestimation of turbulent eddy diffusivities of about a factor 2 for highly turbulent regimes. As some measured dissipation rates were very high, this could be a possible source of error.
Assuming the flux Richardson number to be constant and therefore $\Gamma = 0.2$ could underestimate or overestimate values for K_ρ. Values for Γ could range between 0.15 and 0.25 and disregarding this variability leads to an error of about 30% as reported by *Inall et al.* [2000]. Instrumental errors for airfoil probe measurement could be large, resulting from assuming spectral isotropic conditions and the integration over a fixed wave number spectrum.
However, the largest error here is most likely resulting from the undersampling of non-linear wave events. This fact is further evident in the large error bounds for diapycnal heat fluxes during wave conditions calculated from bootstrap. As wave events were highly variable in intensity as well as spatial and temporal occurrence, the few observed non-linear wave events analysed here might not represent actual conditions in the region. Especially the coverage of background fluxes seems biased, as overall heat fluxes in the background state seem a little too high.

5.4 Outlook

To better quantify the impact of non-linear internal waves on the mixed-layer heat budget on the Peruvian continental shelf, more measurements need to be made. Especially the coverage with microstructure measurements while non-linear internal waves were present during M92 was sparse, at best. Moored profilers, like the McLane Moored Profiler[2], could be of great importance for future observations and measurements as they offer depth profiles of hydrographic conditions and velocities with relatively high temporal

[2] *www.mclanelabs.com/master_page/product-type/profilers/mclane-moored-profiler;* last visited on May 20^{th} 2014

resolution. Gliders, equipped with microstructure sondes, could also be a way to go here. To better capture the spatial and temporal evolution of shoreward propagating non-linear internal waves, they could be tracked from their generation spot to the cost using an array of moorings, as described by *Apel and Holbrook* [1985]. Tracking non-linear internal waves with high-frequency echosounder and ADCP backscatter, as done in the shelf region off New Jersey, by *Shroyer et al.* [2010] and off the coast of Oregon, by *Moum et al.* [2007], and sampled directly and repeatedly as they are approaching the coast would not only lead to a better estimate of background as well as wave conditions, but would also allow a better temporal description of the development of diapycnal heat fluxes as the waves approach the shore. This would result in a more in-depth and statistically significant comparison than this work was able to offer.

A comparison between different seasons would help to further assess the impact of non-linear internal waves in the area, as a seasonal variability in occurrences and intensities of these wave events is likely[3], also reported on the Malin shelf by *Inall et al.* [2001].

[3] *An Atlas of Oceanic Internal Solitary Waves: Northwest South America (Feb 2004) www.internalwaveatlas.com;* last visited on May 20^{th} 2014

6 References

Albert, A., V. Echevin, M. Lévy, and O. Aumont (2010), Impact of nearshore wind stress curl on coastal circulation and primary productivity in the Peru upwelling system, *Journal of Geophysical Research*, *115*(C12), C12,033, doi:10.1029/2010JC006569.

Apel, J. (1995), Internal solitons in the ocean, *Woods Hole Oceanog. Inst. Tech. Rept.*, *WHOI-2006-*.

Apel, J., and J. Holbrook (1985), The Sulu Sea Internal Soliton Experiment, *Journal of Physical Oceanography*.

Barry, M. E., G. N. Ivey, K. B. Winters, and J. Imberger (2001), Measurements of diapycnal diffusivities in stratified fluids, *Journal of Fluid Mechanics*, *442*, 267–291, doi:10.1017/S0022112001005080.

Brink, K., D. Halpern, A. Huyer, and R. Smith (1983), The Physical Environment of the Peruvian Upwelling System, *Progress in Oceanography*, *12*, 285–305.

Chaigneau, A., N. Dominguez, G. Eldin, L. Vasquez, R. Flores, C. Grados, and V. Echevin (2013), Near-coastal circulation in the Northern Humboldt Current System from shipboard ADCP data, *Journal of Geophysical Research: Oceans*, *118*(10), 5251–5266, doi:10.1002/jgrc.20328.

Dewitte, B., S. Illig, L. Renault, K. Goubanova, K. Takahashi, D. Gushchina, K. Mosquera, and S. Purca (2011), Modes of covariability between sea surface temperature and wind stress intraseasonal anomalies along the coast of Peru from satellite observations (2000–2008), *Journal of Geophysical Research*, *116*(C4), C04,028, doi:10.1029/2010JC006495.

Echevin, V., O. Aumont, J. Ledesma, and G. Flores (2008), The seasonal cycle of surface chlorophyll in the Peruvian upwelling system: A modelling study, *Progress in Oceanography*, *79*(2-4), 167–176, doi:10.1016/j.pocean.2008.10.026.

Foltz, G. R., S. A. Grodsky, J. A. Carton, and M. J. McPhaden (2003), Seasonal mixed layer heat budget of the tropical Atlantic Ocean, *Journal of Geophysical Research*, *108*(C5), 3146, doi:10.1029/2002JC001584.

Gregg, M. (1998), Estimation and geography of diapycnal mixing in the stratified ocean, *Physical Processes in Lakes and Oceans*, *54*(section 2), 305–338.

Gregg, M. (1999), Uncertainties and Limitations in Measuring ..., *Journal of Atmospheric & Oceanic Technology*, pp. 1483–1490.

Hallock, Z. R., J. Small, J. George, R. L. Field, and J. C. Scott (2000), Shoreward propagation of internal waves at the Malin Shelf edge, *Continental Shelf Research*, *20*(15), 2045–2057, doi:10.1016/S0278-4343(00)00058-3.

Henyey, F., and A. Hoering (1997), Energetics of borelike internal waves, *Journal of Geophysical Research*, *102*(96), 3323–3330, doi:10.1029/96JC03558.

Hummels, R., M. Dengler, and B. Bourlès (2013), Seasonal and regional variability of upper ocean diapycnal heat flux in the Atlantic cold tongue, *Progress in Oceanography*, *111*, 52–74, doi:10.1016/j.pocean.2012.11.001.

Inall, M., T. Rippeth, and T. Sherwin (2000), Impact of nonlinear waves on the dissipation of internal tidal energy at a shelf break, *Journal of Geophysical . . .*, *105*, 8687–8705.

Inall, M., G. Shapiro, and T. Sherwin (2001), Mass transport by non-linear internal waves on the Malin Shelf, *Continental Shelf Research*, *21*(13-14), 1449–1472, doi:10.1016/S0278-4343(01)00020-6.

Ivey, G., K. Winters, and J. Koseff (2008), Density Stratification, Turbulence, but How Much Mixing?, *Annual Review of Fluid Mechanics*, *40*(1), 169–184, doi:10.1146/annurev.fluid.39.050905.110314.

Jackson, C., J. da Silva, and G. Jeans (2013), Nonlinear internal waves in synthetic aperture radar imagery, *Oceanography*, *26*(2), 68–79.

Klymak, J. M., and J. N. Moum (2003), Internal solitary waves of elevation advancing on a shoaling shelf, *Geophysical Research Letters*, *30*(20), 2045, doi:10.1029/2003GL017706.

Lamb, K. (2003), Shoaling solitary internal waves: on a criterion for the formation of waves with trapped cores, *Journal of Fluid Mechanics*, *478*, 81–100, doi:10.1017/S0022112002003269.

Lamb, K. G. (2014), Internal Wave Breaking and Dissipation Mechanisms on the Continental Slope/Shelf, *Annual Review of Fluid Mechanics*, *46*(1), 231–254, doi:10.1146/annurev-fluid-011212-140701.

Moum, J., and D. Farmer (2003), Structure and generation of turbulence at interfaces strained by internal solitary waves propagating shoreward over the continental shelf., *Journal of Physical . . .*, pp. 2093–2112.

Moum, J. N. (1996), Efficiency of mixing in the main thermocline, *Journal of Geophysical Research*, *101*(C5), 12,057, doi:10.1029/96JC00508.

Moum, J. N., D. M. Farmer, E. L. Shroyer, W. D. Smyth, and L. Armi (2007), Dissipative

Losses in Nonlinear Internal Waves Propagating across the Continental Shelf, *Journal of Physical Oceanography*, *37*(7), 1989–1995, doi:10.1175/JPO3091.1.

Munk, W. (1981), Internal Waves and Small-Scale Processes, *Evolution of physical oceanography*.

Oakey, N. (1982), Determination of the Rate of Dissipation of Turbulent Energy from Simultaneous Temperature and Velocity Shear Microstructure Measurements, *Journal of Physical Oceanography*.

Osborn, T. (1980), Estimates of the local rate of vertical diffusion from dissipation measurements, *Journal of Physical Oceanography*.

Penven, P. (2005), Average circulation, seasonal cycle, and mesoscale dynamics of the Peru Current System: A modeling approach, *Journal of Geophysical Research*, *110*(C10), C10,021, doi:10.1029/2005JC002945.

Pinkel, R., M. Merrifield, M. McPhaden, J. Picaut, S. Rutledge, D. Siegel, and L. Washburn (1997), Solitary waves in the western equatorial Pacific Ocean, *Geophysical Research Letters*, *24*(13), 1603–1606, doi:10.1029/97GL01610.

Sandstrom, H., and J. a. Elliott (2011), Production, transformation, and dissipation of energy in internal tides near the continental shelf edge, *Journal of Geophysical Research*, *116*(C4), C04,004, doi:10.1029/2010JC006296.

Sandstrom, H., and N. Oakey (1995), Dissipation in Internal Tides and Solitary Waves, *Journal of Physical Oceanography*.

Schafstall, J., M. Dengler, P. Brandt, and H. Bange (2010), Tidal-induced mixing and diapycnal nutrient fluxes in the Mauritanian upwelling region, *Journal of Geophysical Research*, *115*(C10), C10,014, doi:10.1029/2009JC005940.

Shih, L. H., J. R. Koseff, G. N. Ivey, and J. H. Ferziger (2005), Parameterization of turbulent fluxes and scales using homogeneous sheared stably stratified turbulence simulations, *Journal of Fluid Mechanics*, *525*(August 2004), 193–214, doi:10.1017/S0022112004002587.

Shroyer, E. L., J. N. Moum, and J. D. Nash (2010), Vertical heat flux and lateral mass transport in nonlinear internal waves, *Geophysical Research Letters*, *37*(8), n/a–n/a, doi:10.1029/2010GL042715.

Small, J., T. Sawyer, and J. Scott (1999), The evolution of an internal bore at the Malin shelf break, *Annales Geophysicae*, *565*(March 1998), 547–565.

Stevenson, J., and P. Niiler (1983), Upper Ocean Heat Budget During the Hawaii-to-Tahiti Shuttle Experiment, *Journal of physical oceanography*.

Thorpe, S. (2007), An introduction to ocean turbulence, *Cambridge University Press*.

Wang, W., and M. McPhaden (1999), The Surface-Layer Heat Balance in the Equatorial Pacific Ocean . Part I : Mean Seasonal Cycle, *Journal of physical oceanography*, pp. 1812–1831.

Acknowledgments

I want to thank Dr Marcus Dengler for the excellent supervision during my thesis and the interesting topic he provided for me. Further, I'd like to thank him for his guidance during my HiWi-job. Without the experience and skills I acquired during my time working for him, analytical work for this thesis would have taken much longer. I'd also like to thank Dr Johannes Karstensen for co-assessing my thesis, and taking me on my first research cruise this summer, directly following my thesis and therefore providing an excellent finish to my undergraduate time at Geomar. Thanks to Carina Minnerup and Alexander Winter for proof-reading and providing tips on text composition.

Very special thanks go out to Eike Köhn, for proof-reading and motivating me to push through the past 2.5 years.

Erklärung

Hiermit erkläre ich, dass ich die vorliegende Arbeit selbständig und ohne fremde Hilfe angefertigt und keine anderen als die angegebenen Quellen und Hilfsmittel verwendet habe.

Die eingereichte schriftliche Fassung der Arbeit entspricht der auf dem elektronischen Speichermedium (benannt mit *1005607.pdf*). Weiterhin versichere ich, dass diese Arbeit noch nicht als Abschlussarbeit an anderer Stelle vorgelegen hat.

Thilo Klenz, Kiel, 3. Juni 2014